Shear wave reflectivity, anisotropies, Poisson's ratios, and densities of a southern Appalachian Paleozoic sedimentary sequence

Joel E. Johnston and Nikolas I. Christensen

Department of Earth and Atmospheric Sciences, Purdue University, West Lafayette, IN 49707, USA

(Received September 11, 1991; revised version accepted May 21, 1992)

ABSTRACT

Johnston, J.E. and Christensen, N.I., 1992. Shear wave reflectivity, anisotropies, Poisson's ratios, and densities of a southern Appalachian Paleozoic sedimentary sequence. *Tectonophysics*, 210: 1–20.

The physical properties of a sequence of Paleozoic sedimentary rocks have been examined in detail, with an emphasis on laboratory measurements of density, shear wave velocity, shear wave splitting, and V_p/V_s ratios. Seismic properties of 147 cores from 49 rock samples collected from the Thorn Hill sedimentary sequence of eastern Tennessee are examined in terms of implications for future seismic studies in the southern Appalachians. The shear wave velocities of these rocks are strongly influenced by the relatively high shear wave velocity of quartz. Shear wave velocity anisotropy is present in most of the lithologic groups; it is highest in the shales while being almost insignificant in the dolostones. The related phenomenon of shear wave splitting occurs to some degree in all of the lithologies studied and at high pressures originates from mineral orientation. Splitting, due to preferred mineral orientation, is most prominent in the shales, but also is significant in some of the carbonates. Compressional to shear velocity (V_p/V_s) ratios of approximately 1.82 (dolostones) and 1.95 (limestones) effectively characterize the carbonates while other lithologies display wider ranges of V_p/V_s, primarily due to the influence of accessory minerals such as quartz. Densities of the sample suite range from 2.34 g/cm^3 (shale) to 2.86 g/cm^3 (dolostone).

Using average data for each lithologic group to calculate normal-incidence reflection coefficients, significant differences in the shear and compressional reflectivity of hypothetical interfaces are found. Normal-incidence shear and compressional wave synthetic seismograms approximating the subsurface reflectivity of the entire Thorn Hill section indicate that three zones of high amplitude reflections would be seen on reflection records obtained over this 3327-m-thick sequence. Overall, the shear and compressional synthetics are similar in appearance. Differences are seen at some interfaces in the Mississippian–Devonian interval, which are more reflective to shear waves, and in the Ordovician Martinsburg Formation, which appears more reflective to compressional waves.

Introduction

Recent seismic studies have seen an increasing use of shear wave reflection and refraction data in conjunction with conventional compressional wave data in the effort to characterize subsurface lithologies and structures. The interest in shear wave velocities is growing in the oil industry (Domenico, 1984; McCormack et al., 1984; Ensley, 1985; Robertson and Pritchett, 1985; Frasier and Winterstein, 1990), as well as in seismic studies of the continental lithosphere (Holbrook et al., 1988; Silver and Chan, 1988; Shih et al., 1991). Shear wave velocities, when combined with compressional wave velocity data, provide valuable constraints on mineralogy, porosity, and anisotropy. In addition, shear wave reflectivity studies have the potential to provide important information on subsurface lithologies and structures.

In recent years, the southern Appalachians have been the focus of several regional, compressional wave seismic reflection studies by the CO-

Correspondence to: J.E. Johnston, Department of Earth and Atmospheric Sciences, Purdue University, West Lafayette, IN. 49707, USA.

CORP (Consortium for Continental Reflection Profiling) and by the ADCOH (Appalachian Ultra Deep Core Hole) project site study in an effort to unravel the tectonic history of the region (e.g., Cook et al., 1979; Brown et al., 1987; Coruh et al., 1987). It has long been believed that the sedimentary rocks exposed in the Valley and Ridge province extend well beneath the crystalline rocks of the Blue Ridge and Piedmont (Bryant and Reed, 1970; Hatcher, 1971, 1972). Continuous, near-horizontal events noted on reflection profiles recorded over the Blue Ridge and Piedmont support this idea (Cook et al., 1979; Coruh et al., 1987) and have led to speculation about the hydrocarbon potential of the overthrust sedimentary strata (Cook et al., 1979; Harris et al., 1981).

Future shear wave seismic exploration efforts, undertaken to explore this possibility and other problems in the southern Appalachians, will require substantial laboratory shear velocity information to constrain data interpretation. The Thorn Hill sedimentary section of eastern Tennessee is an ideal field area for a study of the shear wave properties of the sedimentary strata of the southern Appalachians. At this location in the Valley and Ridge province, almost the entire Paleozoic sedimentary sequence of the southern Appalachians is exposed in a thoroughly studied stratigraphic section (Walker, 1985).

In this paper, we examine the seismic properties of the Thorn Hill section in detail, with an emphasis on the shear wave characteristics of the various lithologies. Velocities have been measured to confining pressures of 200 MPa in order to approximate conditions at depths of up to 7 km. The effect of mineralogy on shear wave velocity is examined. The cause of significant shear wave anisotropy observed in many samples, especially shales, is investigated as well as the related phenomenon of shear wave splitting. Estimating mineral composition from compressional to shear velocity (V_p/V_s) ratios of the Thorn Hill rocks is discussed, along with factors influencing this important parameter. The shear and compressional reflectivities of idealized lithologic interfaces, as calculated from our data, are compared and differences in reflectivity between the two wave domains are examined. Lastly, shear wave synthetic seismograms of the Paleozoic strata of the Thorn Hill section as it would be seen in a normal-incidence shear wave reflection survey are presented and analyzed in detail. These synthetics are then compared to compressional wave synthetics of the same section produced by Christensen and Szymanski (1991).

Experimental technique

Geologic overview and sample collection

Samples for this study were collected from the Thorn Hill stratigraphic section, which is part of the Valley and Ridge province of Eastern Tennessee (Fig. 1). The Thorn Hill section, which is considered by geologists to be one of the classic Paleozoic stratigraphic sections of the southern Appalachians (Walker, 1985), is exposed along a 13-km stretch of highway 25E about 50 miles northeast of Knoxville. The stratigraphy of the Thorn Hill section is presented in Figure 2, along with the stratigraphic locations of the samples collected for this study. The sequence begins in the shales, sandstones, and carbonate units of the Cambrian Rome Formation, which is overlain by limestones and shales of the Conasauga Group. Above this lies a thick sequence of carbonates in the Maynardville Formation, which contains both limestone and dolostone units, and the Cambro-Ordovician Knox Group, an 800-m-thick dolo-

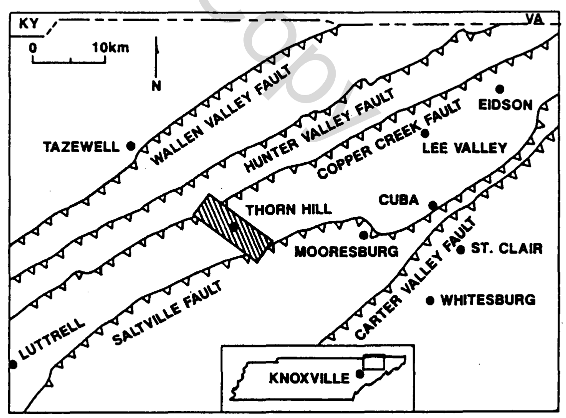

Fig. 1. Simplified map of the Valley and Ridge faults showing Thorn Hill section location.

stone sequence. An unconformity separates the Knox from the lower Chickamauga Group, which is comprised mainly of limestone with some shale units. Overlying the Chickamauga Group are the Ordovician Moccasin and Martinsburg Formations, which consist mainly of limestone, shale, and silty-shale. The top of the Thorn Hill sequence is dominated by clastic rocks in the form of shales, silty-shales, and sandstones. This upper section includes the siltstones and sandstones of the Ordovician Juniata Formation, the Silurian Clinch Sandstone, and the Devonian–Mississippian Chattanooga and Grainger Formations, which are comprised mainly of shales and siltstones, with minor sandstone units (Walker, 1985).

Sample preparation and data collection

Rock samples collected for physical property measurements were oriented in the field. In the laboratory, three mutually perpendicular cores (A, B, and C) roughly 5 cm long were removed from each sample using a 2.54-cm diameter coring bit. The A cores were taken perpendicular to the bedding plane while B and C cores were taken in the bedding plane of each rock, parallel to strike and dip respectively. The ends of the cores were then ground flat and parallel to within 0.008 cm of one another. The lengths, diameters, and weights of the samples were measured so that sample velocity and density could be deter-

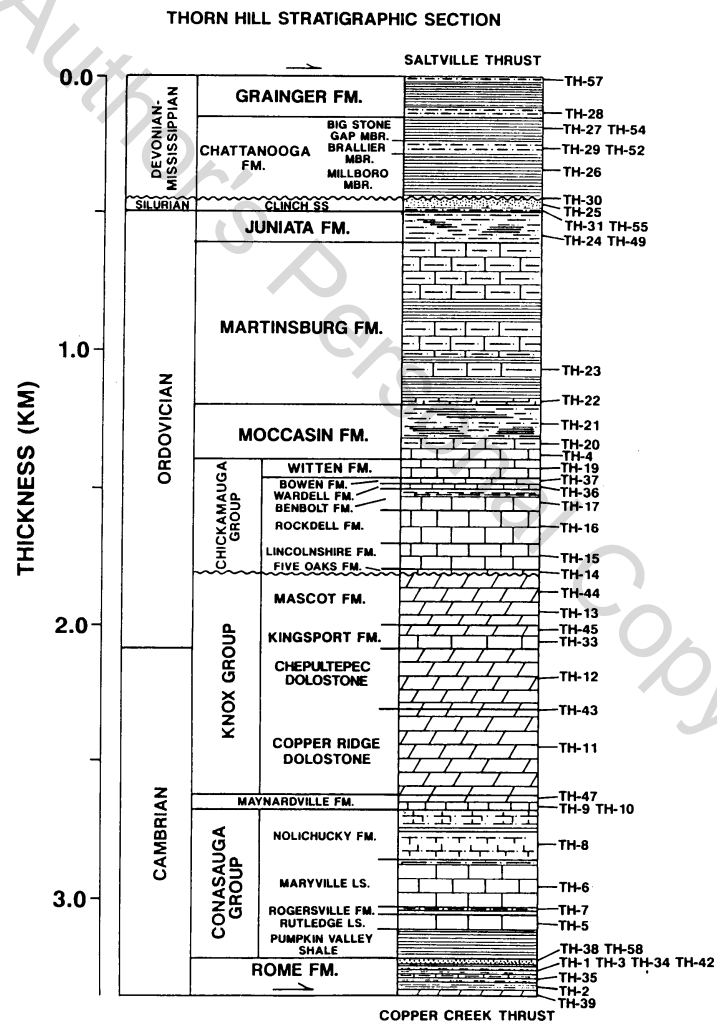

Fig. 2. Stratigraphy of the Thorn Hill sedimentary sequence and sample locations (after Christensen and Szymanski, 1991).

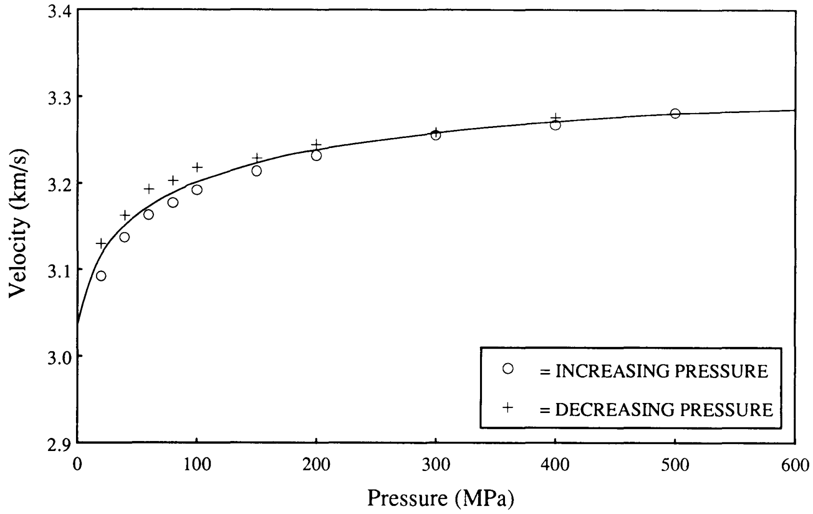

Fig. 3. Shear wave velocity as a function of pressure for sample TH-9.

mined. The effective porosity of each rock was determined by weighing the cores while dry, saturating them in water for 48 hours, then weighing them again to find the weight and volume of the water held in the pore spaces and hence the sample porosity.

Travel times of compressional and shear waves through the samples were measured using the pulse transmission technique (Birch, 1960; Christensen, 1985) and transducers with resonant frequencies of 1 MHz. Velocity determinations were made at hydrostatic confining pressures up to 500 MPa on unsaturated samples, with oil as the confining medium. Velocities measured using this method are considered to be accurate to within 1% (Christensen, 1985).

Orientation of the shear wave vibration direction with the rock fabric is a critical parameter in the laboratory measurement of shear wave anisotropy (Christensen, 1966). In this study, three velocity–pressure measurements were taken per rock sample. In A-core measurements, shear wave vibration directions were aligned parallel to the marked relative orientation of the B cores. In B-core velocity measurements, the shear wave vibration directions were set parallel to bedding. Finally, the shear wave vibration directions were set perpendicular to bedding in either the B or C cores in a third velocity measurement.

A typical shear wave velocity versus pressure curve is illustrated in Figure 3. The rapid increase in velocity up to a confining pressure of about 200 MPa, and subsequent slow increase at higher pressures, is due to closure of rock microcracks at low pressure (Birch, 1961). At a given pressure, a velocity measured at decreasing confining pressure tends to be higher than one measured at increasing pressure. This phenomenon is velocity hysterisis, and is caused by rock inelasticity (Birch, 1960).

Results: physical properties

Shear wave velocities

The 49 sedimentary rock samples collected for this study provide an excellent representation of the lithologic diversity of the Thorn Hill sequence. Sandstones, limestones, dolostones, and shales, as well as intermediate lithologies, are represented in the sample suite. Difficulty was encountered in recovering shales due to weathered outcrops and the fissility of the samples which hindered their collection and coring. Nevertheless, several shales were recovered that have provided important velocity information.

Compressional wave characteristics of the Thorn Hill sequence were reported previously by

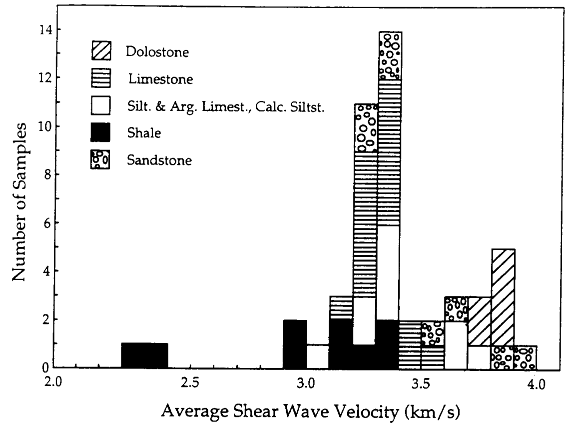

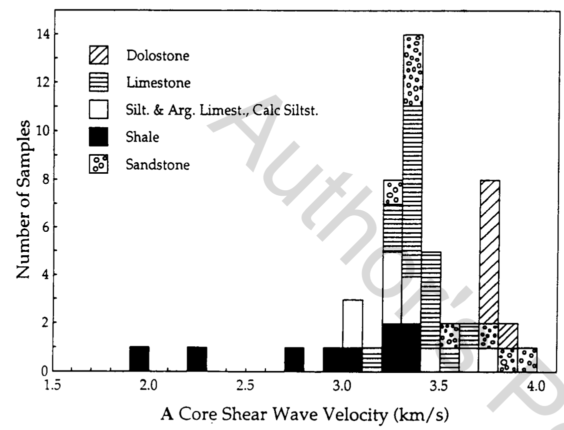

Fig. 4. Average shear wave velocities and shear wave velocities normal to bedding (A cores) at 200 MPa.

Christensen and Szymanski (1991) and will not be discussed here except in relation to shear wave data. Shear and compressional wave velocities, shear and compressional wave anisotropies, densities, and sample descriptions are listed in Table 1. Densities of the samples range from 2.339 g/cm^3 (shale) to 2.838 g/cm^3 (dolostone). Porosities of these extremely well indurated rocks are typically very low, averaging less than 2%. Only the sandstones contain significant porosity, with a sample from the Wildcat Valley Sandstone having the highest porosity at 6.4%.

The sedimentary rocks believed to be overthrust by the Blue Ridge and Piedmont are buried at depths of 6–7 km where confining pressure is approximately 200 MPa. Average and A core shear wave velocity data at 200 MPa for all samples is displayed in Figure 4. Shear wave velocities of the samples range from 1.93 km/s for propagation normal to bedding in a shale (TH-26) to over 3.9 km/s in a dolomitic sandstone (TH-43). Dolostones and limestones have narrow distributions of velocities – between 3.7 and 3.9 km/s and 3.2 and 3.5 km/s, respectively. Other lithologies display wider distributions of velocities. Average sandstone velocities range from 3.2 to 4.0 km/s; shales and siltstones from 2.2 to 3.4 km/s; and argillaceous and silty limestones, and calcareous siltstones from 3.0 to 3.8 km/s.

Several factors are responsible for the velocity distribution noted in Figure 4, the most important being the amount of quartz present in the samples. Pure quartz has a relatively high shear velocity ($V_s = 4.09$ km/s, Voight Reuss Hill average) compared to other common sedimentary rock forming minerals such as calcite (3.36 km/s) and muscovite (3.33 km/s) (Christensen, 1966; Simmons and Wang, 1971). The shear wave velocity of quartz will cause, for example, a silty limestone to have a higher shear velocity than a quartz-free limestone (Wilkens et al., 1984). Velocity scatter could also be due to the presence of other accessory minerals, such as dolomite and clay (Christensen and Szymanski, 1991). The broad distribution of sandstone velocities can be linked to the differing porosities of the samples as well as to their mineralogy (Domenico, 1984).

An average shear wave velocity versus density plot of all samples except the sandstones is displayed in Figure 5. The data define a rough increasing velocity with density trend. The dolostones, with velocities and densities averaging 3.75 km/s and 2.82 g/cm^3, form a distinct velocity–density field, as do the pure limestones. The calcareous siltstones and silty limestones also group fairly well, with the exception of two samples with quartz content over 40% that have velocities near 3.7 km/s. Siltstone and silty-shale samples also exhibit some scatter due to their variable quartz content. In Figure 6, sandstone samples have been added to the plot and a first order, least-squares fit line has been drawn through the non-sandstone samples. The sandstones are extremely scattered and have higher shear velocities at a given density than do the other samples. Porosities and quartz contents are plotted next to the sandstones. As expected, pure

TABLE 1

Summary of physical property data for the Thorn Hill sedimentary sequence. Sample velocities are mean of three measurements per rock

Sample	Lithology	Density (g/cm^3)	Porosity (%)	Pressure = 50 MPa		Pressure = 100 MPa		Pressure = 200 MPa		Pressure = 500 MPa		Anisotropy (%) at 200 MPa	
				V_p (km/s)	V_s (km/s)	V_p (km/s)	V_s (km/s)	V_p (km/s)	V_s (km/s)	V_p (km/s)	V_s (km/s)	V_s	V_p
TH-1	SLS	2.709	0.4	5.98	3.60	6.11	3.65	6.20	3.68	6.30	3.71	2.7	2.2
TH-2	ALS	2.703	1.3	5.49	2.95	5.64	3.01	5.80	3.08	6.02	3.19	3.9	2.8
TH-3	LS	2.697	0.3	6.05	3.21	6.34	3.29	6.48	3.34	6.59	3.37	7.2	1.8
TH-4	LS	2.709	0.4	6.28	3.21	6.32	3.22	6.37	3.23	6.44	3.25	6.0	3.6
TH-5	LS	2.708	0.1	6.51	3.32	6.54	3.33	6.57	3.34	6.61	3.35	5.0	2.7
TH-6	LS	2.723	0.1	6.45	3.32	6.50	3.34	6.55	3.36	6.60	3.37	3.6	1.4
TH-7	LS	2.746	0.1	6.48	3.35	6.57	3.38	6.66	3.40	6.74	3.43	3.4	4.3
TH-8	CSI	2.687	0.6	5.88	3.28	5.97	3.31	6.06	3.35	6.18	3.41	8.0	3.8
TH-9	SLS	2.732	0.5	6.06	3.24	6.16	3.28	6.27	3.33	6.42	3.38	4.3	3.4
TH-10	LS	2.796	0.8	6.18	3.46	6.30	3.49	6.43	3.53	6.64	3.58	0.6	1.2
TH-11	DOL	2.838	0.4	6.74	3.77	6.94	3.82	7.07	3.86	7.20	3.89	2.8	3.9
TH-12	DOL	2.817	0.8	6.59	3.68	6.77	3.75	6.89	3.80	7.02	3.85	2.7	2.1
TH-13	LS	2.690	0.7	6.40	3.10	6.49	3.14	6.55	3.15	6.60	3.17	19.6	1.0
TH-14	LS	2.726	0.2	6.35	3.33	6.41	3.36	6.48	3.38	6.57	3.40	0.9	1.8
TH-15	LS	2.708	0.1	6.31	3.23	6.43	3.26	6.50	3.28	6.58	3.30	3.7	1.3
TH-16	LS	2.696	0.7	6.10	3.13	6.24	3.19	6.35	3.23	6.44	3.29	2.7	0.7
TH-17	LS	2.712	0.3	5.98	3.18	6.19	3.23	6.37	3.26	6.51	3.29	5.5	1.2
TH-19	LS	2.708	0.1	6.33	3.30	6.38	3.32	6.43	3.34	6.49	3.36	0.9	1.0
TH-20	ALS	2.704	0.5	6.16	3.19	6.24	3.21	6.33	3.24	6.41	3.28	1.3	0.1
TH-21	ASI	2.676	1.3	5.12	2.85	5.28	2.89	5.45	2.96	5.68	3.06	3.5	1.7
TH-22	LS	2.714	0.2	6.24	3.18	6.31	3.22	6.38	3.24	6.46	3.25	13.0	5.0
TH-23	SLS	2.712	0.3	6.02	3.25	6.09	3.29	6.16	3.32	6.25	3.37	4.4	6.2
TH-24	ASI	2.696	1.5	5.04	3.00	5.31	3.10	5.54	3.20	5.79	3.31	9.9	3.1
TH-25	SS	2.578	1.9	4.84	3.14	5.29	3.45	5.59	3.66	5.86	3.81	6.8	1.6
TH-26	SH	2.339	1.0	4.09	2.12	4.23	2.18	4.42	2.21	4.73	2.39	39.4	31.4
TH-27	SI	2.580	1.9	4.98	3.09	5.13	3.18	5.31	3.29	5.56	3.41	8.2	6.5
TH-28	ASI	2.653	1.5	5.02	3.14	5.23	3.24	5.44	3.34	5.71	3.45	3.7	4.0
TH-29	SH	2.360	1.2	4.18	2.20	4.36	2.28	4.55	2.38	4.85	2.54	50.1	31.3
TH-30	SS	2.436	6.4	4.50	3.08	4.82	3.19	5.05	3.30	5.29	3.40	3.0	0.3
TH-31	SI	2.683	3.8	4.90	3.05	5.17	3.18	5.44	3.30	5.73	3.43	3.3	4.4
TH-32	ALS	2.702	0.3	5.60	3.11	5.76	3.16	5.92	3.21	6.12	3.27	0.4	5.7
TH-33	SLS	2.792	1.5	6.08	3.50	6.28	3.58	6.47	3.66	6.68	3.74	2.8	5.0
TH-34	SLS	2.720	0.5	6.14	3.65	6.23	3.69	6.32	3.72	6.41	3.74	1.2	2.7
TH-35	LS	2.707	0.9	5.97	3.19	6.09	3.22	6.21	3.25	6.35	3.29	9.2	11.6
TH-36	ALS	2.716	0.8	5.71	3.16	6.03	3.24	6.30	3.31	6.51	3.36	2.1	0.7
TH-37	LS	2.723	0.5	6.55	3.39	6.60	3.40	6.63	3.41	6.66	3.42	1.0	2.2
TH-38	SS	2.592	1.7	5.49	3.22	5.32	3.31	5.81	3.37	5.98	3.43	6.5	10.5
TH-39	DOL	2.863	0.3	6.70	3.66	6.81	3.70	6.89	3.73	7.00	3.76	0.6	0.8
TH-42	LS	2.710	0.1	6.34	3.31	6.36	3.32	6.39	3.33	6.44	3.35	0.1	0.4
TH-43	DSS	2.731	0.1	6.17	3.78	6.39	3.88	6.51	3.91	6.63	3.94	1.1	2.0
TH-44	DOL	2.792	0.9	6.69	3.71	6.82	3.77	6.90	3.80	6.99	3.83	1.1	2.5
TH-45	DOL	2.805	0.7	6.71	3.71	6.89	3.79	6.98	3.82	7.08	3.85	1.1	2.5
TH-47	DOL	2.812	0.9	6.49	3.63	6.59	3.67	6.68	3.70	6.79	3.74	0.7	1.8
TH-49	SI	2.664	1.8	5.10	2.99	5.24	3.06	5.40	3.15	5.67	3.28	3.3	3.8
TH-52	SS	2.490	4.6	4.52	2.95	4.71	3.09	4.94	3.25	5.24	3.43	2.1	2.9
TH-54	SISH	2.546	0.9	4.48	2.74	4.65	2.82	4.86	2.92	5.18	3.05	8.4	9.3
TH-55	SS	2.554	2.4	5.06	3.56	5.40	3.78	5.58	3.90	5.76	3.99	7.0	1.7
TH-57	SS	2.653	1.2	5.19	3.36	5.37	3.45	5.55	3.54	5.77	3.64	0.6	1.8
TH-58	SS	2.597	1.5	5.24	3.19	5.50	3.30	5.69	3.39	5.88	3.46	4.0	5.5

[1] DOL = dolostone; LS = limestone; SLS = silty limestone; ALS = argillaceous limestone; CSI = calcareous siltstone; ASI = argillaceous siltstone; SI = siltstone; SS = sandstone; DSS = dolomitic sandstone; SH = shale; SISH = silty shale.

sandstones of low porosity display higher shear velocities than those with larger amounts of impurities and porosity (Domenico, 1984).

Shear wave anisotropy

Seismic anisotropy can result from a number of factors, the most significant being large- and small-scale stratigraphic layering, preferred orientation of minerals, and alignment of cracks and pores (Christensen, 1966; Carlson and Christensen, 1979; Jones and Wang, 1981; Crampin, 1985). In laboratory rock velocity measurements, closure of microcracks occurs at hydrostatic confining pressures near 200 MPa (Birch, 1961). Anisotropy observed at higher pressures can be attributed to preferred orientation of minerals. In sedimentary rocks, this is referred to as lithologic anisotropy, which occurs when individual grains are aligned with the bedding plane during deposition or by deformational processes shortly afterwards.

In multi-core laboratory rock velocity measurements, seismic anisotropy is defined as the difference between the maximum and minimum rock velocity (as determined from the three cores taken per rock) expressed as a percentage of the mean rock velocity (Birch, 1960). A histogram displaying shear wave anisotropy of the Thorn Hill rocks at 200 MPa is given in Figure 7. The dolostones, with anisotropies less than 4%, appear to be almost isotropic to shear waves. Limestones, argillaceous and silty limestones, and sandstones display slightly higher anisotropy on average. Surprisingly, several limestones have significant anisotropy, up to 19% in one sample. Carbonate rock anisotropy can be attributed to preferred orientation of accessory clay minerals, or even alignment of the calcite or dolomite grains themselves (Christensen and Szymanski, 1991).

Shales and argillaceous siltstones display the largest anisotropies of all the Thorn Hill rocks. Anisotropy of these clastic rocks can be attributed to their high clay content and preferential alignment of the highly anisotropic clay minerals with the bedding plane (Jones and Wang, 1981). For these rocks, the velocity of the shear wave propagating in the bedding plane and vibrating parallel to bedding is generally greater than that of the shear wave propagating in the bedding plane but vibrating perpendicular to bedding. This finding is consistent with the observation that most shales, in the absence of aligned cracks or pores, can be considered transversely isotropic with the main symmetry axis perpendicular to bedding (Jones and Wang, 1981; Rai and Hanson, 1988).

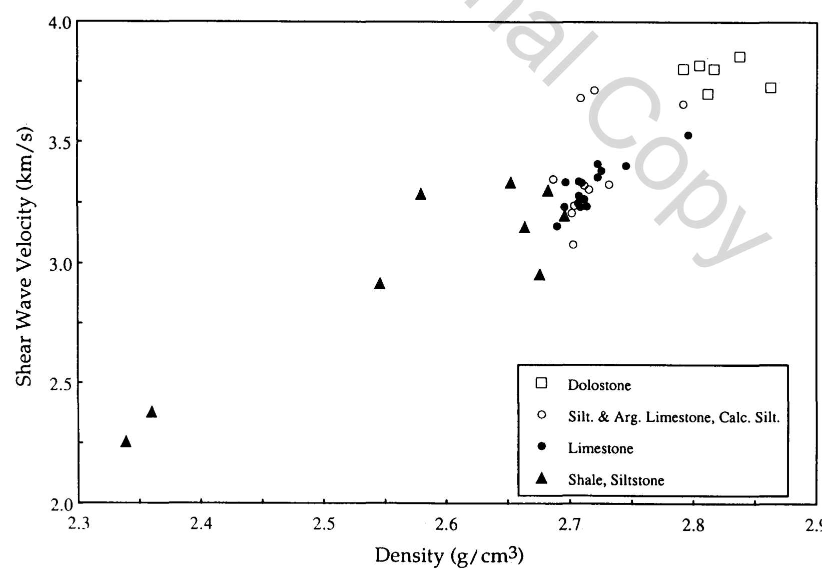

Fig. 5. Shear wave velocity–density data at 200 MPa for all samples except sandstones.

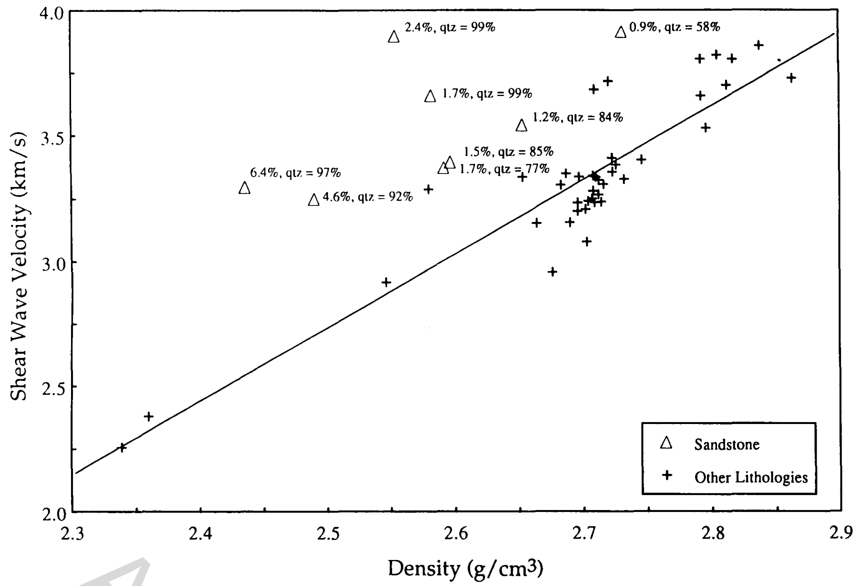

Fig. 6. Velocity–density data of Figure 5 with sandstone data added. First-order least-squares line fit is for non-sandstone samples. Porosities and quartz contents are shown for sandstones (see text).

Shear wave splitting

In field exploration seismology, examining subsurface anisotropy through the use of compressional wave data requires two or more azimuthally different propagation paths. Shear waves, due to the phenomenon of shear wave splitting, can provide velocity anisotropy information using a single propagation direction. Upon entering an anisotropic medium, a single shear wave will be vectorially split into two orthogonally polarized components which travel along the same propagation path with different velocities (Christensen, 1966, 1971). The fast wave will have a vibration direction parallel to cracks at low pressures and be controlled by mineral orientation at high pressures. Upon arriving at a receiver in the field, or a transducer in the laboratory, the polarization direction of the fast shear wave and the time delay between the split arrivals can be evaluated to determine the nature of the anisotropic medium. Thus, shear waves provide an additional source of lithologic information not provided by compressional wave studies of the same medium (Crampin, 1985).

To investigate shear wave splitting produced by mineral alignment in the Thorn Hill section, two shear wave velocities were measured per B core for seventeen rock samples. B cores, as mentioned previously, were taken parallel to bedding. The velocities of the shear waves vibrating parallel (S_{par}) and perpendicular (S_{per}) to bedding were measured for each of these cores. Differences in these velocities for a given B core indicates shear wave splitting, most likely caused by preferential mineral alignment. Figure 8 is a plot of S_{par} versus S_{per} velocity in the bedding plane at 200 MPa confining pressure for the

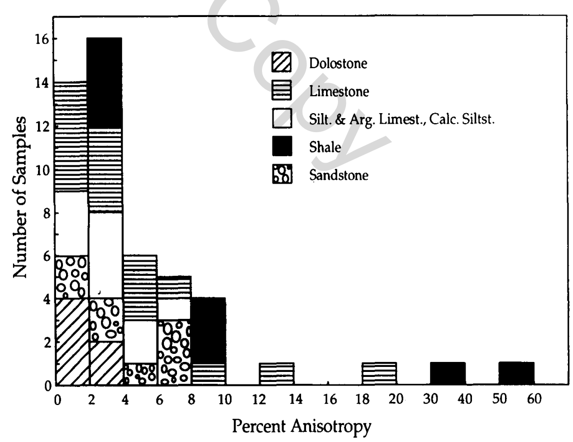

Fig. 7. Shear wave velocity anisotropy of sample suite at 200 MPa.

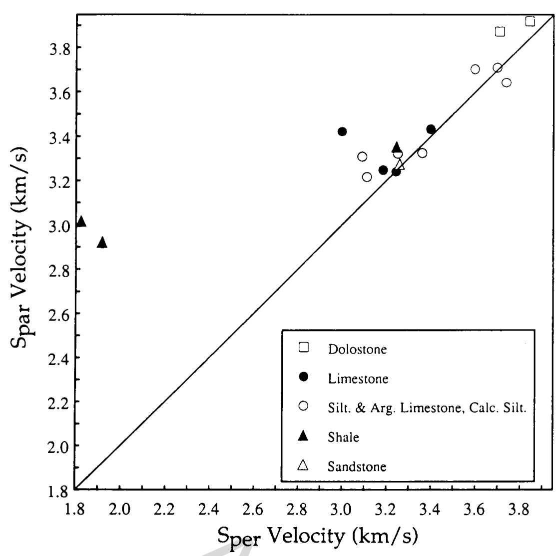

Fig. 8. Shear wave velocities for vibration directions parallel to bedding (S_{par}) versus shear wave velocities for vibration directions perpendicular to bedding (S_{per}).

seventeen samples. A line representing equal velocities, or zero shear wave splitting is also given. Shear wave splitting is noticed in many of the samples, including the carbonates. S_{par} wave velocity in the bedding plane is higher than the S_{per} wave velocity for almost all of the samples, a result of mineral alignment parallel to bedding (Christensen, 1966; Jones and Wang, 1981). Figure 9 is a graphical display of the time differences between the fast and slow shear waves for each of the 17 samples assuming wave propagation through 300 m of material under confining pressures of 50, 200, and 400 MPa. Time differences between the fast and slow shear arrivals range from 0.3 ms in a limestone to 78.5 ms in a shale taken from the Braillier member of the Chattanooga Shale. No overall trend can be seen between changes in confining pressure and the degree of splitting in the samples. Variations in the time delay between the fast and slow arrivals with increasing pressure can, however, be attributed to a decreasing contribution to overall sample anisotropy by rock microcracks (Baud, 1988). This microcrack influence can be seen in the data of the two shale samples of Figure 9.

Kaarsberg (1959) in his study of natural and artificial aggregates found that preferred orientation of submicroscopic platy clay minerals occurs parallel to bedding, which results in strong bonding and elasticity parallel to bedding and weak

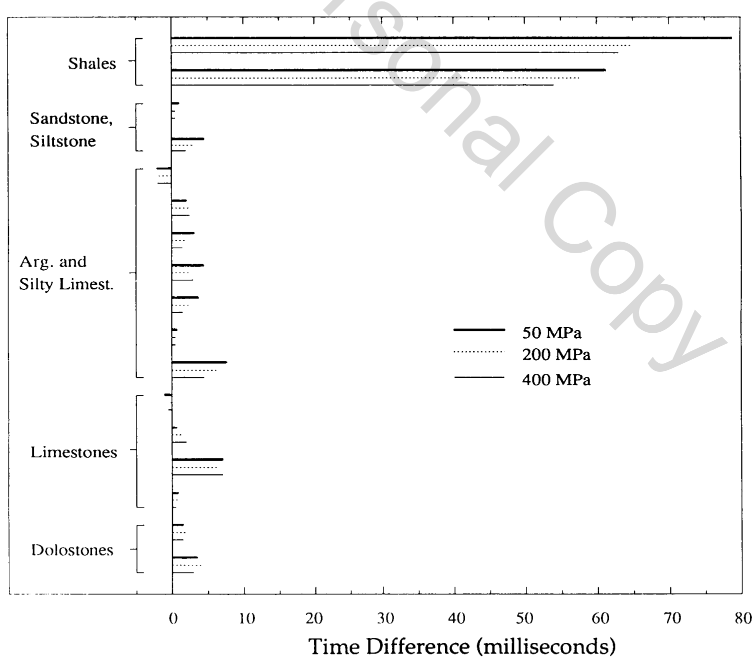

Fig. 9. Representation of time differences between S_{par} and S_{per} waves of Figure 8 assuming propagation through 300 m of rock material. Lines to the right of the vertical axis indicate a faster S_{par} than S_{per} velocity.

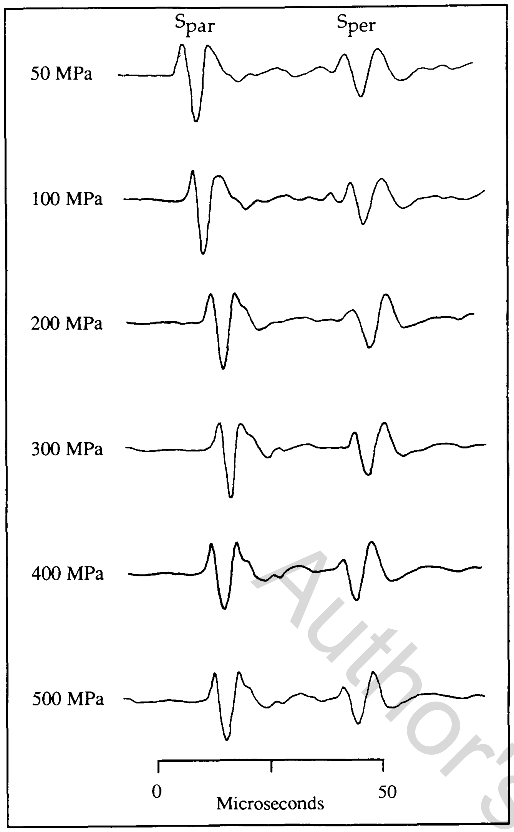

Fig. 10. Graphical representation of shear wave splitting produced by shale sample TH-26 as seen on oscilloscope screen at various confining pressures.

bonding and inelasticity perpendicular to bedding. Thus, a shear wave propagating in the bedding plane of a shale vibrating parallel to bedding travels much faster than a shear wave vibrating perpendicular to bedding with the same propagation direction. In order to further investigate the magnitude of shear wave splitting produced by the shales, a core taken in the bedding plane of sample TH-26 (Chattanooga Shale) was subjected to an additional velocity–pressure measurement. In this procedure, the transducer vibration direction was oriented at an angle of 45 degrees to the bedding plane to induce shear wave splitting. Figure 10 is a graphical representation of the traces displayed on the oscilloscope screen using this technique at confining pressures between 50 and 500 MPa. Note the large time separation between the fast (vibrating parallel to bedding) and slow (vibrating perpendicular to bedding) shear arrivals produced by propagation through a core approximately 4 cm long. The time difference between the fast and slow arrivals appears to decrease slightly with increasing confining pressure, probably due to closure of rock microcracks.

Compressional to shear velocity ratios (V_p / V_s)

The ratio of compressional to shear wave velocity (V_p/V_s) is important in seismological studies for discriminating between subsurface lithologies and structures (Macelwane, 1951; Christensen and Fountain, 1975; Tatham and Stoffa, 1976; Tatham 1982; Domenico, 1984; Wilkens et al., 1984; Castagna et al., 1985; Eastwood and Castagna, 1986). For example, McCormack et al. (1984) examined the lateral variation in V_p/V_s of the gas producing Morrow Formation of New Mexico and used this variation to identify changes in the sand to shale ratio of the unit. Robertson (1987) examined lateral changes in V_p/V_s of a carbonate hydrocarbon producing horizon and used this parameter to identify lateral changes in porosity and pore content. Holbrook et al. (1988), in a more regional study, produced a petrologic model of the lower crust of southwestern Germany using Poisson's ratios (calculated from V_p/V_s) obtained from refraction data.

In order that future shear and compressional wave seismic reflection studies of the southern Appalachians are provided with interpretational constraints, V_p/V_s values for the Thorn Hill sequence are presented in Figure 11. Average compressional and shear wave velocities for each rock

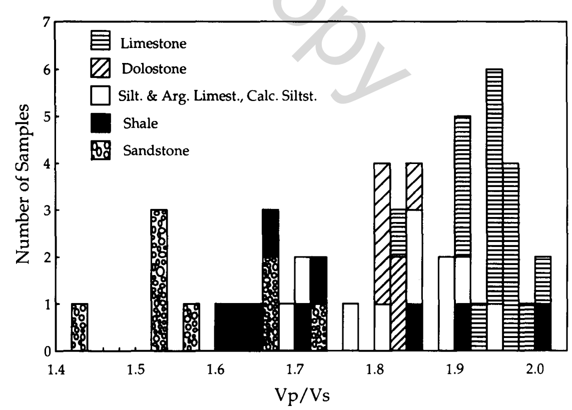

Fig. 11. V_p / V_s of the Thorn Hill sample suite at 200 MPa.

at 200 MPa confining pressure were used to produce this histogram. The pure carbonates are characterized well by this parameter. Dolostone V_p/V_s ranges from 1.8 to 1.86, with a peak in the interval 1.81–1.82, a result which agrees with an average V_p/V_s of 1.8 for this lithology reported by McCormack et al. (1984). Values of V_p/V_s given in the literature for limestones range from 1.71 to as high as 2.75, with an average value of 1.9 (McCormack et al., 1984). V_p/V_s of the Thorn Hill limestones ranges from 1.9 to 2.2, with a peak between 1.94 and 1.98. V_p/V_s of the silty limestones, argillaceous limestones, and calcareous siltstones displays a range of values from 1.68 to 1.96, primarily due to their variable quartz content. Those rocks with a significant quartz content will have a lower V_p/V_s than rocks with lesser quartz due to the high shear wave velocity of this mineral (Wilkens et al., 1984).

Sandstone V_p/V_s reported in the literature ranges from 1.5 to 1.9, with unsaturated sandstones having a V_p/V_s around 1.5 (McCormack et al., 1984). The Thorn Hill sandstones display a considerable range of V_p/V_s, from 1.42 to 1.7, a phenomenon which requires some explanation. Studies of water-saturated sandstones indicates that both porosity and clay content increase V_p/V_s, with porosity having the greater effect (Eastwood and Castagna, 1986). As expected, the three sandstones (TH-25, 30, 55) of this study with quartz contents near 99% have low values of V_p/V_s (1.53 or below). Those with greater amounts of accessory minerals have higher values of V_p/V_s. Velocity measurements in this study were taken under unsaturated conditions and on a limited range of porosities; therefore, no conclusions can be drawn concerning sample porosity and pore fluid and their effect on V_p/V_s of sandstones.

The two pure shales examined in this study, TH-26 and TH-29, have V_p/V_s values of 2.00 and 1.91, respectively. McCormack et al. (1984) reported in situ V_p/V_s for shales ranging from 2.43 to 2.7, while noting that laboratory determined values are typically much lower. *In situ* shales are saturated to some degree, a condition which would increase the compressional wave velocity (and decrease the shear wave velocity) relative to an unsaturated sample and, therefore, increase V_p/V_s relative to an unsaturated sample.

A different presentation of V_p/V_s in the Thorn Hill sample suite is given in Figure 12, in which the mean V_p/V_s of the samples is plotted as a function of mean shear wave velocity. Error bars representing one standard deviation are also given. This plot emphasizes the narrow ranges of

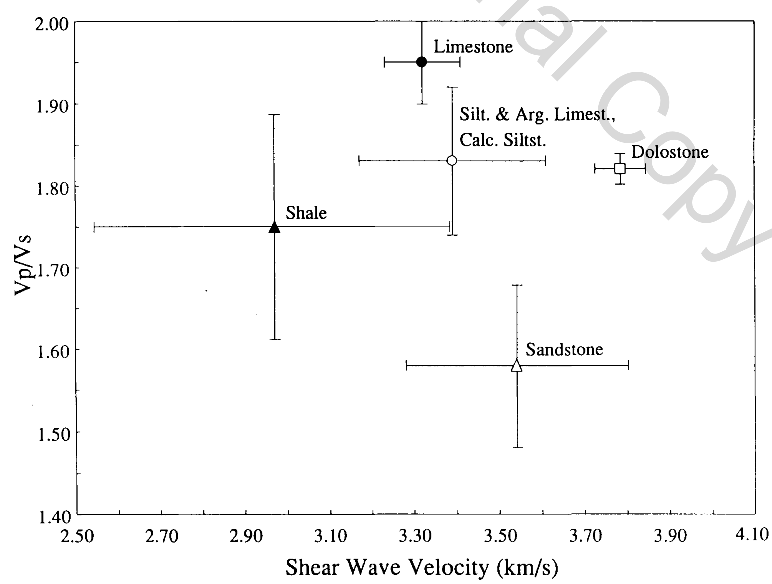

Fig. 12. Plot of average V_p/V_s versus average shear wave velocity for the lithologic groups at 200 MPa.

the shear velocities and V_p/V_s of the pure carbonates and the wider ranges of these values in the other lithologic groups. Considerable overlap of V_p/V_s for the shales and siltstones, impure limestones and calcareous siltstones, and sandstones is noted.

In Figure 13, V_p/V_s of the Thorn Hill samples at 200 MPa confining pressure are plotted against V_p/V_s of the same samples at 50 MPa, a pressure at which porosity in the form of rock microcracks should have a strong effect on velocities (Birch, 1961). A line representing equal V_p/V_s is also given. V_p/V_s of most of the samples is greater at 200 MPa. Wilkens et al. (1984) studied the effects of confining pressure on V_p/V_s of unsaturated silty limestones and found that changes in V_p/V_s with pressure could be related to the pore geometry of the samples. Closure of low aspect ratio pores (thin cracks) between 50 and 200 MPa would increase shear wave velocities more than compressional wave velocities, resulting in a decrease of V_p/V_s with increasing pressure. High aspect ratio pores probably do not close over this pressure range, but decrease in volume, resulting in an overall increase in V_p/V_s (Toksoz et al., 1976; Wilkens et al., 1984). Thus, Figure 13 shows that in the pressure range 50–200 MPa, low aspect ratio pores are nearly all closed and changes

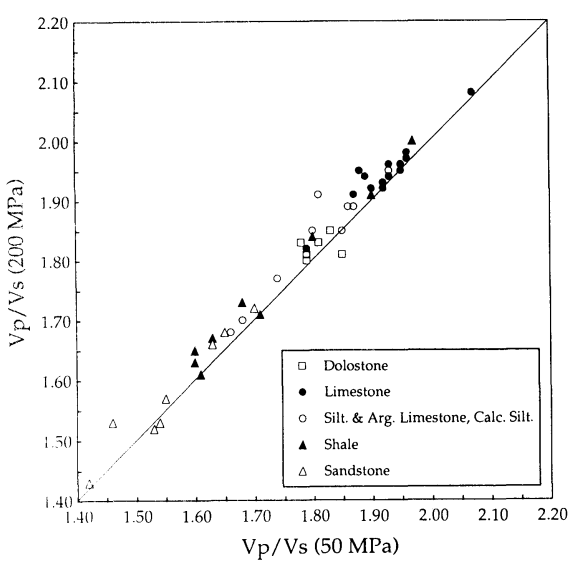

Fig. 13. V_p/V_s of sample suite at 200 MPa versus V_p/V_s at 50 MPa.

in V_p/V_s for the majority of the Thorn Hill rocks can be attributed to the effects of confining pressure on high aspect ratio pores.

Results: reflectivity

The formulas for the normal-incidence compressional and shear wave reflection coefficients are as follows:

$$R_p = (\rho_2 v_2 - \rho_1 v_1)/(\rho_2 v_2 + \rho_1 v_1)$$

$$R_s = (\rho_1 v_1 - \rho_2 v_2)/(\rho_2 v_2 + \rho_1 v_1)$$

where ρ_1 and v_1 are the density and velocity, respectively, of the medium overlying the interface and ρ_2 and v_2 are that of the medium below the interface (e.g., Aki and Richards, 1980). The shear wave reflection coefficient differs from the compressional wave formula only by a sign change in the numerator, which is necessary for continuity of displacement and stress across the interface. The shear wave reflection coefficient for a given lithologic contact can correspond to a positive, negative, or zero magnitude compressional reflection coefficient for the same interface. If V_p/V_s remains the same across an interface R_p and R_s will be of the same magnitude but of opposite sign. Usually, however, V_p/V_s will vary considerably in the subsurface due to the wide range of lithologies and corresponding ranges of velocity possible. Therefore, coincident shear and compressional reflection sections can vary considerably in character even after careful processing designed to facilitate comparison (McCormack et al., 1984).

Model interfaces

Normal-incidence shear wave reflection coefficients for various hypothetical lithologic contacts have been calculated from the average densities and A-core shear wave velocities (representing normal incidence) of the dolostones, limestones, sandstones, and siltstones. For clarity, the signs or polarities of these reflection coefficients will be ignored. The shales produce large reflection coefficients when placed in contact with other lithologies due to their low velocity for propaga-

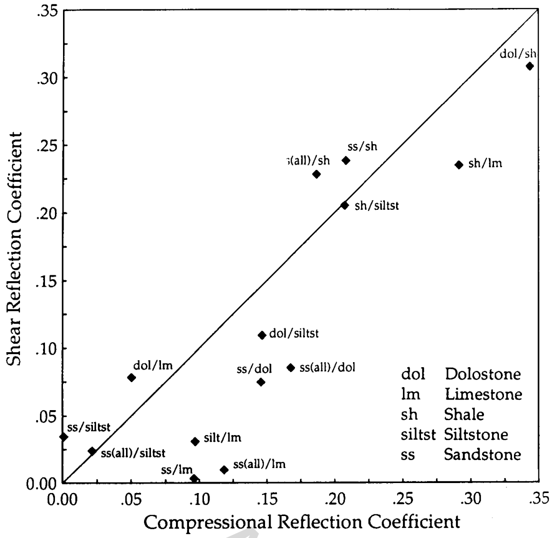

Fig. 14. Plot of normal incidence shear versus compressional reflection coefficients (absolute values) produced by various lithologic contacts using averaged lithologic data.

tion paths normal to bedding and their low density. Especially large shear wave reflection coefficients result from shale/ dolostone (0.31), shale/limestone (0.23), and sandstone/shale (0.23) interfaces. Slightly smaller reflection coefficients are produced by dolostone/sandstone (0.09), dolostone/siltstone (0.11), and dolostone/ limestone (0.08) interfaces while siltstone/ limestone (0.03), sandstone/siltstone (0.02), and sandstone/limestone (0.01) contacts result in small impedance contrasts.

Figure 14 is a comparison of shear and compressional normal-incidence reflection coefficients (absolute values) of these interfaces. A line representing equal shear–compressional reflectivity is also given. Note that due to the highly variable shear wave velocities and densities of the sandstones, two sandstone groups are plotted, one including all sandstone samples and another consisting of four samples with self-consistent porosity and density.

Several observations can be made from this plot. First, it can be seen that under unsaturated conditions, a sandstone/limestone interface is much more reflective to compressional waves than to shear waves. The average compressional wave velocity and density of the sandstone samples is 5.37 km/s and 2.58 g/cm^3, compared to 6.41 km/s and 2.72 g/cm^3 for the limestones. Both the density and compressional wave velocity of the limestones are higher than the corresponding values for the sandstones, resulting in a relatively strong compressional wave impedance contrast. The average shear wave velocity of the sandstones (3.54 km/s), however, is significantly higher than that of the limestones (3.32 km/s) due to the quartz content of the sandstones. Thus, the difference in the shear wave velocities offsets the large difference in density between these rocks, resulting in a relatively small impedance contrast for shear waves. These sandstones, the only lithology in this study to have significant porosity, are almost certainly saturated to some degree in the subsurface. In Figure 15, compressional and shear wave impedances calculated from the A-core data of sandstone sample TH-55 (porosity of 2.44%) are plotted as a function of confining pressure. Unsaturated and saturated data are given. At confining pressures of approximately 150 MPa and above, compressional and shear impedances show no significant changes between dry and saturated conditions. Thus, at relatively high confining pressures, saturation has little effect on the model reflectivity results.

A sandstone/dolostone interface appears to be more reflective to compressional waves than to shear waves. This reflectivity contrast is similar to that discovered in the sandstone/limestone case

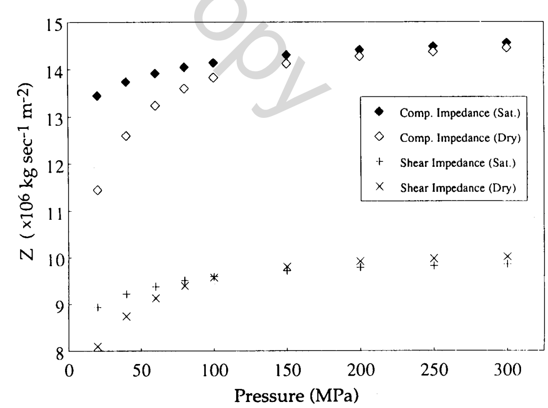

Fig. 15. Compressional and shear impedances (Z) of sandstone sample TH-55 as a function of confining pressure.

and the explanation for it is the same. Dolostone/siltstone and limestone/siltstone interfaces also appear to be more reflective to compressional waves. In contrast to the observations made so far, a dolostone/limestone contact, when using averaged lithologic data, appears slightly more reflective to shear waves. No conclusions will be drawn regarding the shales due to the limited amount of data available for this lithology.

Shear wave synthetic seismograms

Future reflection surveys in the southern Appalachians will require physical property information in order to tie shear wave reflection data to the known stratigraphy of the area, and to correlate seismic events on coincident shear–compressional profiles. Synthetic seismograms used to approximate the reflectivity of the Paleozoic rocks of the Thorn Hill sequence in the subsurface can be helpful in this regard. In this section, shear wave synthetic seismograms of the Thorn Hill section are presented which have been calculated using the velocity–density data derived from this study.

A total of 63 layers were used to approximate, in detail as great as possible, the 3327-m-thick sequence in the seismic modeling. Unit thicknesses were taken from the Walker (1985) Thorn Hill guidebook. The rock samples and layer representations are the same as those used by Christensen and Szymanski (1991), with newly collected samples incorporated. At locations where

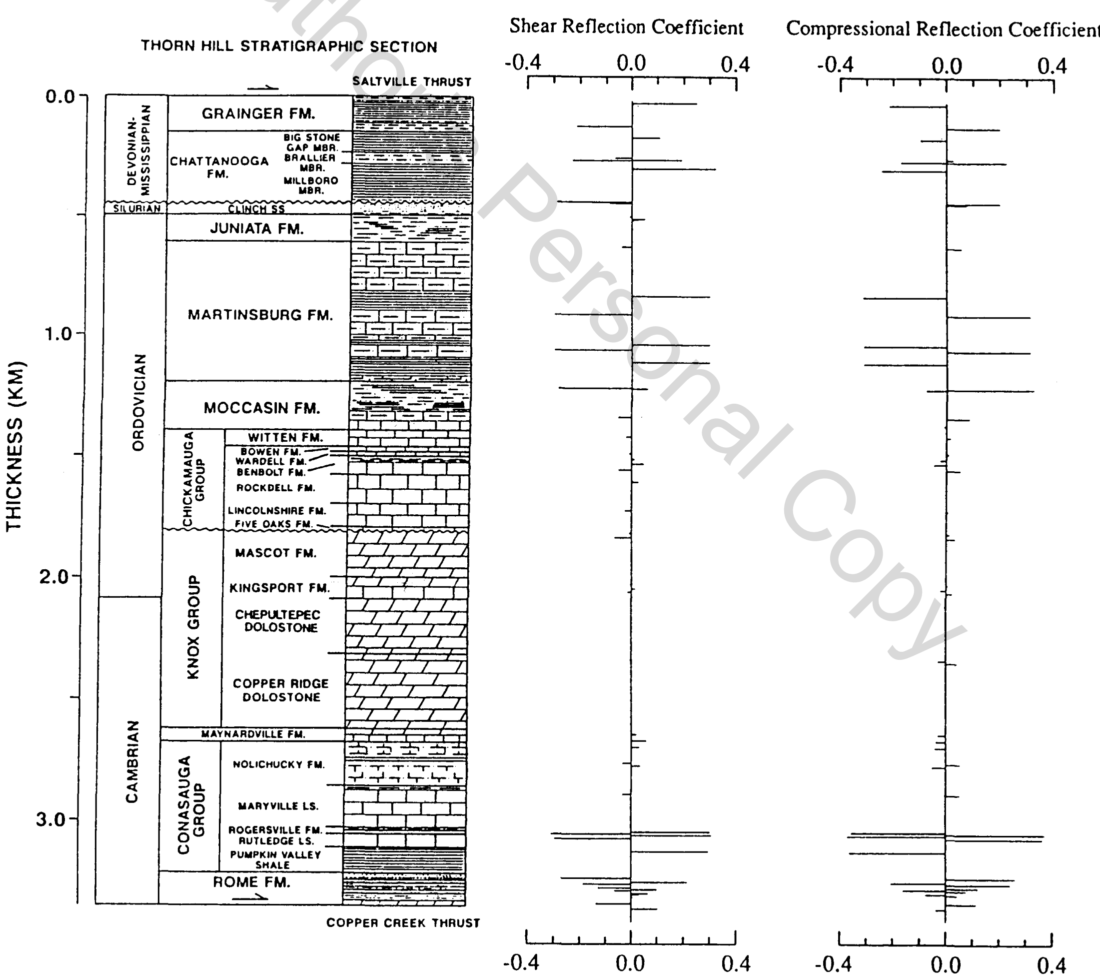

Fig. 16. Thorn Hill sedimentary sequence along with shear and compressional reflection coefficients (200 MPa data) at interfaces.

sample coverage was lacking, lithologies present were approximated using average lithologic data. Shear and compressional A-core velocities (approximating normal incidence) measured at 200 MPa were used in the modeling process.

Figure 16 is a plot of the shear and compressional wave reflection coefficients, as generated by the above model, as a function of depth. The shear and compressional spike plots both seem to indicate that three areas of high-amplitude events could be expected on reflection profiles of a subsurface Thorn Hill section. The uppermost zone corresponds to the alternating shales, siltstones, and sandstones of the Mississippian Grainger Formation and the Devonian Chattanooga Shale, the middle zone corresponds with the alternating shales and limestones of the Ordovician Martinsburg Formation, and the lowermost zone with the alternating shales and limestones of the lower Conasauga Group and the varied lithologies of the Cambrian Rome Formation. The Ordovician Moccasin Formation and the Chickamauga Group produce smaller impedance contrasts, as do the Cambrian upper Conasauga Group and Maynardville Formation. It appears that the largely carbonate Knox Group would not be reflective to shear or compressional waves. These findings agree with those published by Christensen and Szymanski (1991).

A normal-incidence shear wave synthetic seismogram of the entire Thorn Hill section is displayed in Figure 17. A gain function has not been applied to the data so that amplitude information can be analyzed directly. This synthetic seismogram was produced by computing a time series containing the shear reflection coefficients given in Figure 16 and convolving it with a Ricker source wavelet having a dominant frequency of 15 Hz. The equivalent vibroseis bandwidth, approximately 1–30 Hz, is commonly used in shear wave surveys (Edelmann and Helbig, 1986; Layotte, 1986). The synthetic seismogram program takes into account transmission losses at interfaces but does not produce multiples or random noise. Since both of these features are attenuated during common depth point processing, however, the synthetics used in this study give a fair representation of near-normal-incidence shear wave and compressional wave reflection survey records (Christensen and Szymanski, 1991). Three highly

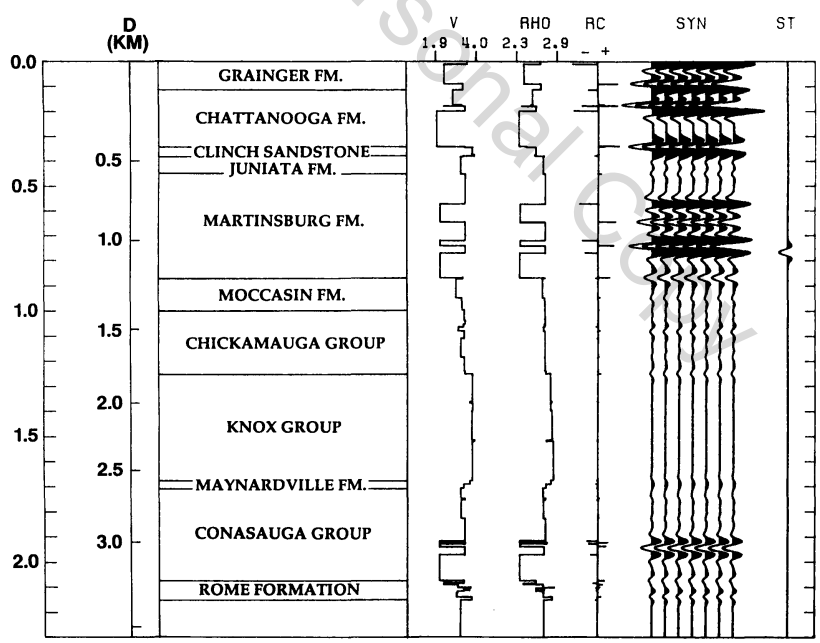

Fig. 17. Normal incidence shear wave synthetic seismogram of the Thorn Hill sequence generated using a 15-Hz Ricker wavelet. Velocity (V), density (RHO), and reflection coefficients (RC) with depth also given.

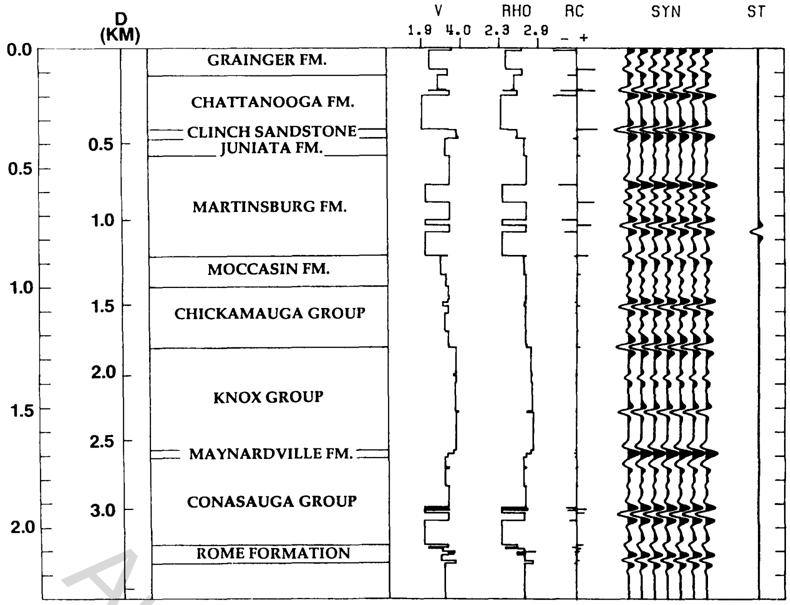

Fig. 18. Normal incidence shear wave synthetic seismogram of Figure 17 after application of an automatic gain function.

reflective sections separated by relatively transparent intervals can be seen on this synthetic. These zones correspond to the Mississippian–Devonian strata, the limestone and shale beds of the Martinsburg Formation, and the lower Conasauga Group and Rome Formation. These results confirm the findings of the reflection coefficient plot of Figure 16.

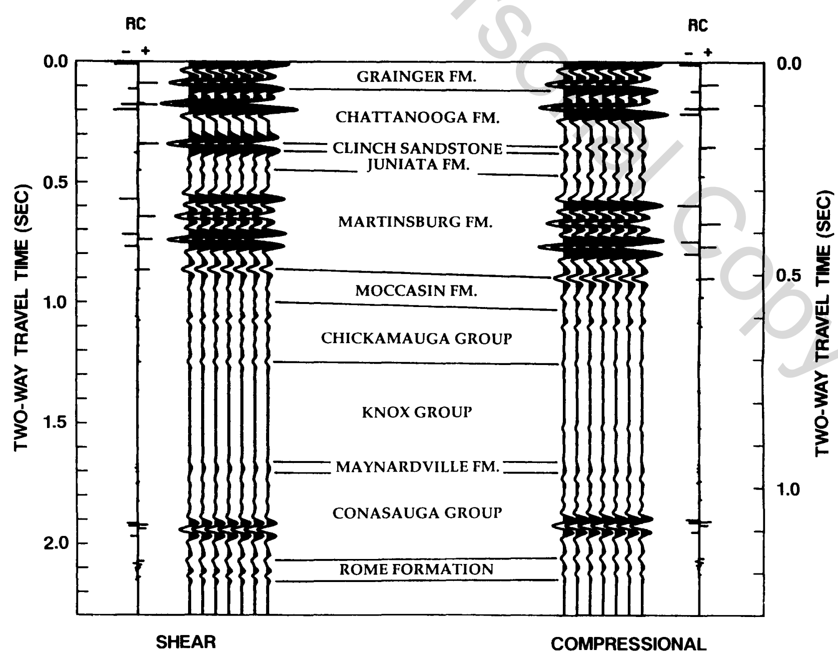

Fig. 19. Comparison of shear wave synthetic seismogram of Figure 17 to compressional wave synthetic seismogram produced using a 25-Hz Ricker wavelet.

Application of an automatic gain function to the data using a 230-ms window (Fig. 18) enhances reflections internal to the Chickamauga Group and at the Chickamauga Group/Knox contact. In addition, two small reflections can now be seen in the Knox Group, one at the Copper Ridge/Chepultepec Formation contact which is marked by minor beds of arenaceous dolostone and dolomitic sandstone (TH-43). The contact of the Knox with the underlying Maynardville Formation is now clearly seen, as is the reflection event at the base of the section.

Comparison of shear and compressional reflectivity

In the last aspect of this study, we compare the shear and compressional wave reflectivity of the Thorn Hill sequence through the use of synthetic seismograms. By noting the response of a subsurface interval to shear and compressional waves, these synthetics can provide useful information for future shear/compressional investigations in the southern Appalachians, mainly in the area of seismic event correlation during coincident surveys.

In Figure 19, the shear wave synthetic of Figure 18 is compared to a compressional wave synthetic of the Thorn Hill section generated using a 25-Hz Ricker wavelet. The equivalent vibroseis bandwidth, approximately 5–50 Hz, is commonly used in compressional wave crustal surveys (Hale and Thompson, 1982; Brown et al., 1987). Gain functions have not been applied so that amplitudes can be analyzed quantitatively. In order that the shear and compressional synthetics can be compared, it is necessary that the vertical resolving power is nearly equal in the wave domains. Vertical resolution in reflection seismology is directly proportional to wavelength (λ) and is defined as the minimum vertical separation between beds such as they can be identified as individual features (Yilmaz, 1987). Widess (1973) found that vertical resolution can be approximated by ($\lambda/8$) in noise free data and ($\lambda/4$) in noisy data. Assuming an average subsurface compressional velocity of 6.3 km/s for the Thorn Hill section, as determined in this study, a 25-Hz wavelet would have a wavelength of 250 m, resulting in a resolving power of 31 m in noise free data. Similarly, an average subsurface shear velocity of 3.3 km/s would result in a 15-Hz wavelet having a wavelength of approximately 220 m, yielding a vertical resolving power of approximately 27 m. Thus, the frequencies used in the generation of these synthetics result in almost equal resolution in the shear and compressional wave domains and direct comparison of the synthetics is valid.

Due to the fact that the normal-incidence shear and compressional reflection coefficients differ by a sign change in the numerator, reflections from the same interface (assuming a constant V_p/V_s across the interface) would be of the same sign but of opposite polarity. To simplify comparison of the sections, the synthetic program has been modified so that positive reflection coefficients are marked by amplitude excursions to the left for both wave types.

The shear and compressional sections of Figure 19 are similar in overall appearance. Important differences are noted, however. Most of these reflectivity contrasts occur in the upper part of the section. For example, the Braillier Siltstone/Millboro Shale contact is more reflective to shear waves ($R_s = 0.32$) than to compressional waves ($R_p = 0.24$). Below this, a major difference in reflectivity is noted at the Chattanooga Shale/Wildcat Valley Sandstone contact. The shear wave reflection ($R_s = 0.29$) occurring at this interface is much stronger than the corresponding compressional reflection ($R_p = 0.20$).

In the middle part of the Thorn Hill section, the alternating shales and limestones of the Ordovician Martinsburg Formation appear slightly more reflective on the compressional wave synthetic. Only minor differences in reflectivity are noted in the section composed of the Moccasin Formation, the Chickamauga Group, and the Knox Group. For example, the upper contact of the Knox with the Chickamauga Group is more easily identified on the shear wave section. In contrast, the dolomitic sandstone layer present at the Chepultepec/Copper Ridge Formation contact produces a weak compressional wave reflection and no shear wave reflection at all. With the addition of noise and short path multiples, as would be present on a processed CDP section taken from field data, the reflectivity differences in the middle part of the section would probably not be noticed.

The Cambrian base of the Thorn Hill section also shows minor differences in reflectivity. The shales and limestones of the lower Maryville Formation, the Rogersville Formation, and the Rutledge Formation produce a slightly stronger composite compressional than shear reflection. In contrast to this, the lower Cambrian Rome Formation and the Copper Creek thrust fault appear slightly more reflective to shear waves than to compressional waves.

Brief mention must be made of the limitations of these synthetic seismograms. For example, random noise and multiples are not generated by the synthetic program used in this study, as mentioned previously. Also, shear wave splitting would be a major factor in a shear wave reflection survey and would affect the character of reflection profiles. The splitting could be induced by aligned, near-vertical cracks caused by tectonic stresses, or by mineral orientation. Both of these features are obviously present in the southern Appalachians. The major characteristics of the synthetic seismograms, however, are likely to be seen on coincident reflection profiles over the Paleozoic rocks exposed in the Thorn Hill section.

Conclusions

The major theme of this paper is that shear wave data provides significant complimentary information when used with compressional wave data to characterize lithologies. The major conclusions of this study are as follows:

(1) Shear wave velocities in the Thorn Hill sedimentary sequence range from 1.93 km/s for propagation perpendicular to bedding in a shale to over 3.91 km/s in a dolomitic sandstone. Densities of the samples range from 2.34 g/cm^3 (shale) to 2.86 g/cm^3 (dolostone).

(2) Quartz, as a primary or secondary mineral, has a strong effect on the shear wave velocities of many of the lithologies examined due to its relatively high shear wave velocity.

(3) Shear wave velocity anisotropy is widespread and significant among the sedimentary rocks of the southern Appalachians. Anisotropy is greatest in the shales and silty shales, but it is also present in many of the other lithologies. Most of the dolostones appear almost isotropic to shear waves.

(4) Shear wave splitting, caused by preferred orientation of minerals, occurs to some degree in almost all of the sedimentary lithologies of the Thorn Hill section. It is most prominent in the shales and silty-shales, but can also be identified in the other lithologies.

(5) The pure carbonates of Thorn Hill are effectively characterized by V_p/V_s. The other lithologies display wider ranges of V_p/V_s due to variations in composition within the given lithologic groups. Change in V_p/V_s with increasing confining pressure can be attributed to closure of pores with various aspect ratios in the samples.

(6) Normal-incidence shear and compressional reflectivity modeling indicates that sandstone/limestone and sandstone/dolostone interfaces are more reflective to compressional waves than to shear waves, while a limestone/dolostone interface appears to be more reflective to shear waves.

(7) Three zones of high-amplitude reflections can be expected on shear and compressional wave reflection profiles over the Paleozoic rocks exposed in the Thorn Hill section. The synthetic seismograms produced in this study also seem to indicate that shear and compressional reflection profiles of the Thorn Hill strata would be similar in overall character. Several interfaces, however, have noticeably contrasting responses to shear and compressional waves, which could prove useful as stratigraphic markers for correlation during future coincident surveys in the southern Appalachians.

Acknowledgements

The assistance of D. Szymanski in earlier phases of this study is appreciated. D. Kingma and S. Lewis made many of the velocity measurements. Laboratory studies were supported by the Office of Naval Research contract N00014–89-J-1209.

References

Aki, K. and Richards, P.G., 1980. Quantitative Seismology: Theory and Methods, Volume 1. W.H. Freeman and Company, New York, N.Y, 557 pp.

Baud, R.D., 1988. Calculating crack density values from compressional and shear wave velocities. M.S. Thesis, Purdue Univ., West Lafayette, Ind., 56 pp.

Birch, F., 1960. The velocity of compressional waves in rocks to 10 kilobars, 1. J. Geophys. Res., 65: 1083–1102.

Birch, F., 1961. The velocity of compressional waves in rocks to 10 kilobars, 2. J. Geophys. Res., 66: 2199–2224.

Brown, L., Wille, D., Zheng, L., Devoogd, B., Mayer, J., Hearn, T., Sanford, W., Caruso, C., Zhu, T., Nelson, D., Potter, C., Hauser, E., Klemperer, S., Kaufman, S. and Oliver, J., 1987. COCORP: New perspectives on the deep crust. Geophys. J.R. Astron. Soc., 89: 47–54.

Bryant, B. and Reed, J.C. Jr., 1970. Geology of the Grandfather Mountain window and vicinity, North Carolina and Tennessee. U.S. Geol. Surv., Prof. Pap. 615, 190 pp.

Carlson, R.L. and Christensen, N.I., 1979. Velocity anisotropy in semi-indurated calcareous deep sea sediments. J. Geophys. Res., 84: 205–211.

Castagna, J.P., Batzle, M.L. and Eastwood, R.L., 1985. Relationships between compressional wave and shear wave velocities in clastic silicate rocks. Geophysics, 50: 571–581.

Christensen, N.I., 1966. Shear wave velocities in metamorphic rocks at pressures to 10 kilobars. J. Geophys. Res., 71: 3549–3556.

Christensen, N.I., 1971. Shear wave propagation in rocks. Nature, 229: 549–550.

Christensen, N.I., 1985. Measurements of dynamic properties of rock at elevated temperatures and pressures. In: H.J. Pincus and E.R. Hoskins (Editors), Measurements of Rock Properties at Elevated Pressures. American Society for Testing and Materials, Philadelphia, Penn., pp. 93–107.

Christensen, N.I. and Fountain, D.M., 1975. Constitution of the lower continental crust based on experimental studies of seismic velocities in granulite. Geol. Soc. Am. Bull., 86: 227–236.

Christensen, N.I. and Szymanski, D.L., 1991. Seismic properties and the origin of reflectivity from a classic paleozoic sedimentary sequence, Valley and Ridge province, southern Appalachians. Geol. Soc. Am. Bull., 103: 277–289.

Cook, F.A., Albaugh, D.S., Brown, L.D., Kaufman, S., Oliver, J.E. and Hatcher, R.D., Jr., 1979. Thin-skinned tectonics in the southern Appalachians: COCORP seismic reflection profiling of the Blue Ridge and Piedmont. Geology, 7: 563–567.

Coruh, C., Costain, J.K., Hatcher, R.D., Jr., Pratt, T.L., Williams, R.T. and Phinney, R.A., 1987. Results from regional Vibroseis profiling: Appalachian ultradeep core hole site study. Geophys. J.R. Astron. Soc., 89: 147–155.

Crampin, S., 1985. Evaluation of anisotropy by shear wave splitting. Geophysics, 50: 142–152.

Domenico, S.N., 1984. Rock lithology and porosity determination from shear and compressional wave velocity. Geophysics, 49: 1188–1195.

Eastwood, R.L. and Castagna, J.P., 1986. Interpretation of Vp/Vs ratios from sonic logs. In: S.H. Danboom and S.N. Domenico (Editors), Shear Wave Exploration. Soc. Explor. Geophys., Geophys. Dev. Ser., 1: 139–153.

Edelmann, H.A.K. and Helbig, K., 1986. Shear wave surveys: some aspects of field layout. In: S.H. Danboom and S.N. Domenico (Editors), Shear Wave Exploration. Soc. Explor. Geophys., Geophys. Dev. Ser., 1: 39–47.

Ensley, R.A., 1985. Evaluation of direct hydrocarbon indicators through comparison of compressional- and shear-wave seismic data: a case study of the Myrnam gas field, Alberta. Geophysics, 50: 37–48.

Frasier, C. and Winterstein, D., 1990. Analysis of conventional and converted mode reflections at Putah sink, California using three component data. Geophysics, 55: 646–659.

Hale, L.D. and Thompson, G.A., 1982. The seismic reflection character of the continental Mohorovicic discontinuity. J. Geophys. Res., 87: 4625–4635.

Harris, L.D., Harris, A.G., DeWitt, W., Jr. and Bayer, K.C., 1981. Evaluation of southern eastern overthrust belt beneath Blue Ridge-Piedmont thrust. Bull. Am. Assoc. Pet. Geol., 65: 2497–2505.

Hatcher, R.D., 1971. Stratigraphic, petrologic, and structural evidence favoring a thrust solution to the Brevard problem. Am. J. Sci., 270: 177–202.

Hatcher, R.D., 1972. Developmental model for the southern Appalachians. Geol. Soc. Am. Bull., 83: 2735–2760.

Holbrook, W.S., Gajewski, D., Krammer, A. and Prodehl, C., 1988. An interpretation of wide-angle compressional and shear wave data in southwest Germany: Poisson's ratio and petrologic implications. J. Geophys. Res., 93: 12,081–12,106.

Jones, L.E.A. and Wang, H.F., 1981. Ultrasonic velocities in Cretaceous shales from the Williston basin. Geophysics, 46: 288–297.

Kaarsberg, E.A., 1959. Introductory studies of natural and artificial argillaceous aggregates by sound propagation and x-ray diffraction methods. J. Geol., 67: 447–472.

Layotte, P.C., 1986. MARTHOR, an S-wave source. In: S.H. Danboom and S.N. Domenico (Editors), Shear Wave Exploration. Soc. Explor. Geophys., Geophys. Dev. Ser., 1: 79–96.

Macelwane, S.J., 1951. Evidence on the interior of the earth developed from seismic sources. In: B. Gutenberg (Editor), Internal Constitution of the Earth. Dover Publ., New York, N.Y., pp. 227–304.

McCormack, M.D., Dunbar, J.A. and Sharp, W.W., 1984. A case study of stratigraphic interpretation using shear and compressional seismic data. Geophysics, 49: 509–520.

Rai, C.S. and Hanson, K.E., 1988. Shear wave velocity anisotropy in sedimentary rocks: A laboratory study. Geophysics, 53: 800–806.

Robertson, J.D., 1987. Carbonate porosity from S/P traveltime ratios. Geophysics, 52: 1346–1354.

Robertson, J.D. and Pritchett, W.C., 1985. Direct hydrocarbon detection using comparative P-wave and S-wave seismic sections. Geophysics, 50: 383–393.

Shih, X.R., Schneider, J.F. and Meyers, R.P., 1991. Polarities of P and S waves, and shear wave splitting observed from the Bucaramanga Nest, Columbia. J. Geophys. Res., 96: 12,069–12,082.

Silver, P.G. and Chan, W.W., 1988. Implications for continental structure and evolution from seismic anisotropy. Nature, 335: 34–39.

Simmons, G. and Wang, H., 1971. Single Crystal Elastic Constants and Calculated Aggregate Properties. Handbook, the MIT Press, Cambridge, Mass., 370 pp.

Tatham, R.H., 1982. V_p/V_s and lithology. Geophysics, 47: 336–344.

Tatham, R.H. and Stoffa, P.L., 1976. V_p/V_s – A potential hydrocarbon indicator. Geophysics, 41: 837–849.

Toksoz, M.N., Cheng, C.H. and Timur, A., 1976. Velocities of seismic waves in porous rocks. Geophysics, 48: 621–645.

Walker, K.R., 1985. The geologic history of the Thorn Hill Paleozoic section (Cambrian–Mississippian) eastern Tennessee. Univ. Tennessee, Dep. Geol. Sci., Studies in Geology 10, 128 pp.

Widess, M.B., 1973. How thin is a thin bed?. Geophysics, 38: 1176–1180.

Wilkens, R., Simmons, G. and Caruso, L., 1984. The ratio V_p/V_s as a discriminant of composition for siliceous limestones. Geophysics, 49: 1850–1860.

Yilmaz, O., 1987. Seismic Data Processing. In: E.W. Neitzel (Editor), Investigations in Geophysics, Volume 2. Society of Exploration Geophysicists, Tulsa, Okla., 526 pp.